PyroCb Detection and Monitoring in Near-Real-Time

US Naval Research Laboratory
Marine Meteorology Division

01 September 2016

1. What are pyroCb?

Smoke plumes from large and intense fires often become capped by cumulus clouds (known as pyroCu, http://glossary.ametsoc.org/wiki/Pyrocumulus), which enhance the vertical lofting of smoke through latent heat release. Under certain conditions, this "pyroconvection" mechanism allows pyroCu to develop into a larger fire-triggered thunderstorm, known as pyrocumulonimbus (or pyroCb, http://glossary.ametsoc.org/wiki/Pyrocumulonimbus). The deep convective column provides an efficient method for lofting smoke particles and gaseous emissions well into the upper troposphere, drastically impacting the extent of downwind transport (Fig. 1). Intense pyroCb activity can also inject a significant quantity of aerosol mass into the lower stratosphere, occasionally more than 7-10 km above the tropopause [*Fromm et al.,* 2005, 2008a,b].

Fig. 1: Intense pyroCb observed in Colorado during June 2013.

2. Viewing PyroCb from Space

As viewed from space, intense pyroconvection is displayed as a cluster of fire pixels adjacent to a cumulus cloud, which is anchored to the fire and oriented downwind. The typical pyroCb life cycle involves initiation in mid-afternoon and termination a few hours after sunset [*Fromm et al.,* 2010]. The pyroCb anvil can be a single, relatively brief feature (e.g., less than one hour) to a multi-hour, multi-pulse cloud, with two or more anvils [*Rosenfeld et al.,* 2007]. Cessation of pyroCb is evidenced by the separation of the cold-cloud feature from the fire pixel cluster and movement downwind. Previous studies have employed a variety of *ad hoc* remote sensing and modeling techniques to identify pyroCb events [*Rosenfeld et al.,* 2007; *Fromm et al.,* 2005, 2008a, 2010]. A selection of pyroCb events identified by these manual techniques during 2014-2016 (Fig. 2, red symbols) demonstrates the geographic range of this phenomenon.

3. The NRL PyroCb Algorithm

The US Naval Research Laboratory (NRL) has developed an algorithm and webpage that systematically detects pyroCb using geostationary satellite observations (http://www.nrlmry.navy.mil/pyrocb-bin/pyrocb.cgi) from the imager onboard GOES-W and GOES-E (4 km nominal pixel size), as well as the Advanced Himawari Imager (AHI, 2 km nominal pixel size) onboard Japan's recently launched Himawari-8 satellite (operational in early 2015), which is nearly identical to the future Advanced Baseline Imager (ABI) onboard GOES-R and GOES-S. This

constellation (Fig. 2) provides coverage several times per hour over the majority of pyroCb-prone regions worldwide using both current and next-generation sensors. PyroCb detection has been successfully demonstrated at viewing zenith angles up to 75°.

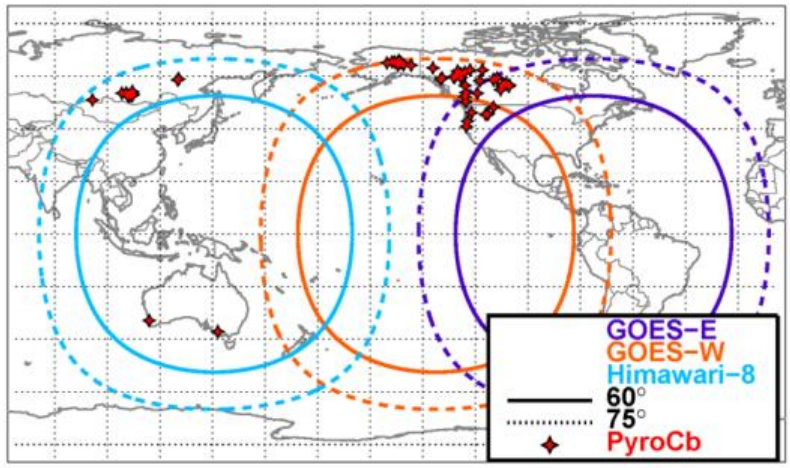

Fig. 2: Coverage from geostationary satellites available from the NRL pyroCb webpage: GOES-East (purple), GOES-West (orange), and Himawari-8 (light blue). Circles indicate the viewing domain of each sensor within a view zenith angle of 60° (solid line) and 75° (dashed line). Symbols show a selection of pyroCb events identified manually during 2014-2016.

Close proximity in space and time to one or more satellite fire detections is the first requirement for pyroCb detections. Intense pyroCb pixels must exhibit a thermal infrared (11 µm) brightness temperature (BT_{11}) below an approximated homogeneous liquid-water freezing threshold (-35 °C) [*Wallace and Hobbs,* 2006; *Rosenfeld et al.,* 2007], thus reflecting a high likelihood of smoke particles approaching the tropopause. Marginal pyroCb pixels must have a BT_{11} less than -20 °C.

Extreme aerosol loading within a pyroCb will induce a microphysical shift (from indirect aerosol effects) toward smaller cloud droplets and ice particles [*Reutter et al.,* 2014, *Chang et al.,* 2015], producing a much larger daytime near-infrared (4 µm) reflectivity than traditional convection [e.g., *Rosenfeld et al.,* 2007]. Application of a 4 and 11 µm brightness temperature difference (BTD_{4-11}) therefore allows for separation of pyroCb from more pristine traditional convection [*Peterson et al.,* in revision, a]. However, the dependence on 4 µm reflectivity currently limits pyroCb detection to daytime scenes (solar zenith angle < 80°). Two BTD_{4-11} thresholds are employed based on regional variability in convective clouds, which is driven by meteorological conditions. A cloud opacity test (BTD_{11-13}) is also included to reduce potential cloud edge noise and detection errors from thin clouds over a hot fire.

The algorithm can detect individual pyroCb events, pyroCb embedded within traditional convection, and multiple, short-lived pulses of activity. A flow chart of the NRL pyroCb detection algorithm, including its input and output, is provided in Fig. 3 and *Peterson et al.* [in revision, a]. A description of the meteorological environment favorable for pyroCb development is provided by *Peterson et al.* [2015] and *Peterson et al.* [in revision, b].

4. NRL PyroCb Webpage Products

PyroCb detection products are available from **three geostationary satellite sensors** (Fig. 2):
GOES-13 (gvar-goesE), GOES-15 (gvar-goesW), and Himawari-8 (ahi-h8).

Three polar-orbiting sensors provide supplementary products:
Terra MODIS (modis-terra), Aqua MODIS (modis-aqua), and S-NPP VIIRS (viirs-npp).

The following table provides the details of each product:

PyroCb Product	Description
PyroCb-Standard	Detection of intense and marginal pyroCb pixels based on the standard cloud microphysics threshold ($BTD_{4\text{-}11}$ > 50°C). MODIS fire pixels (MOD/MYD14) are also provided in native resolution (~1.0 km).
PyroCb-High-LCL	Detection of intense and marginal pyroCb pixels based on a cloud microphysics threshold ($BTD_{4\text{-}11}$ > 60°C) for a high lifting condensation level (LCL) environment (high cloud bases). This product is applicable when the LCL temperature is less than 0°C, roughly coincident with an LCL height of 3000 m AGL (Fig. 3). MODIS fire pixels (MOD/MYD14) are also provided in native resolution (~1.0 km).
11µm	Longwave infrared brightness temperature, with color shading indicating the deep convection (BT_{11} < -20 °C) and ice cloud (BT_{11} < -35 °C) thresholds (Fig. 3).
4µm	Shortwave infrared brightness temperature. PyroCb will have unusually large values compared to routine opaque ice clouds.
4-11BTD	Brightness temperature difference (BTD) between the short (4 µm) and longwave (11 µm) infrared channels, with color shading indicating cloud microphysics. A pyroCb anvil must have at least one pixel meeting the standard microphysics threshold ($BTD_{4\text{-}11}$ > 50°C). The high-LCL threshold ($BTD_{4\text{-}11}$ > 60°C) is also applied when the LCL temperature is less than 0°C, roughly coincident with an LCL height of 3000 m AGL (Fig. 3).
11-13BTD	Brightness temperature difference (BTD) between the 11 and 13 µm infrared channels, with color shading indicating cloud opacity. A pyroCb must have an optically thick anvil, coinciding with $BTD_{11\text{-}13}$ values less than 3.0°C (Fig. 3).

Supplementary	Description
Visible	Visible imagery is available from all sensors.
True-Color	Available from Terra/Aqua MODIS and S-NPP VIIRS.
Night-Vis-IR	Imagery from the VIIRS Day-Night Band, including an infrared overlay.

5. Algorithm Sensitivity and Limitations

Small anvil size in comparison the large pixel size of geostationary sensors (2-4 km nominal resolution) is the primary cause of missed detections, especially in in regions with large viewing angles (larger pixel sizes). The NRL algorithm therefore primarily detects large and intense pyroCb events [*Peterson et al.,* in revision, a]. Although the algorithm is sensitive to traditional convection with extreme updraft velocities (e.g., large convective available potential energy), this situation is uncommon during pyroCb development [*Peterson et al.*, in revision, b]. Algorithm assessment also reveals potential sensitivity to traditional convection that has ingested a large quantity of smoke particles from nearby fires. Geostationary sensors only detect cloud top temperature, and therefore cannot provide information on vertical structure below the cloud top.

5.1 Western Siberia Anomaly at Sunset

$BTD_{4\text{-}11}$ often becomes very large for cloud cover observed in western Siberia at sunset. This anomaly results from specular reflection (sunglint) in areas where the solar and sensor zenith angles are similar and the relative azimuth is high.

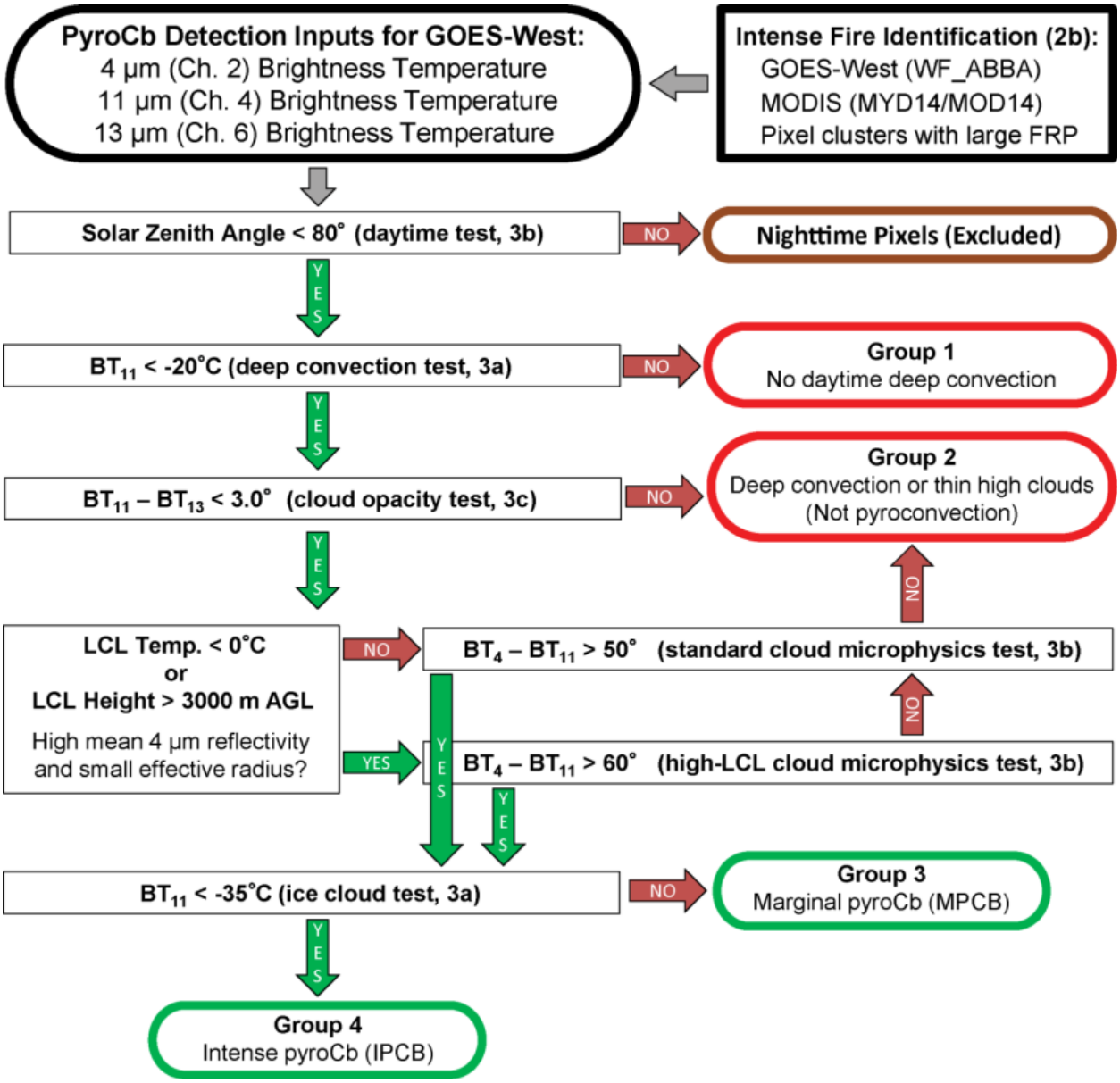

Fig. 3. Flowchart of the NRL pyroCb detection algorithm (daytime only), with the four output groups highlighted in red or green ovals. Each algorithm step also includes the number of the section where it is described in Peterson et al. [in revision, a].

6. Disclaimer

This is an official U.S. Navy Algorithm and Website.

Usage: Our image products are freely available to the general public for noncommercial use. We require proper acknowledgment that is found at http://www.nrlmry.navy.mil/linknotice.htm.

No Guarantee: The satellite-based products produced here at NRL are experimental in nature and targeted for near-real-time application; therefore, NRL is not responsible for the accuracy of its contents. The products are free to the public. However, if any images are displayed elsewhere, please reference Naval Research Laboratory - Monterey.

7. Resources and References

PyroCb Community Discussion Group:
https://groups.yahoo.com/neo/groups/pyrocb/info

CIMSS PyroCb Blog:
http://pyrocb.ssec.wisc.edu/

Chang, D., and Coauthors, 2015: Comprehensive mapping and characteristic regimes of aerosol effects on the formation and evolution of pyro-convective clouds. *Atmospheric Chemistry and Physics*, **15,** 10325-10348.

Fromm, M., R. Bevilacqua, R. Servranckx, J. Rosen, J. P. Thayer, J. Herman, and D. Larko, 2005: Pyro-cumulonimbus injection of smoke to the stratosphere: Observations and impact of a super blowup in northwestern Canada on 3-4 August 1998. *Journal of Geophysical Research-Atmospheres*, **110**.

Fromm, M., and Coauthors, 2008a: Stratospheric impact of the Chisholm pyrocumulonimbus eruption: 1. Earth-viewing satellite perspective. *Journal of Geophysical Research-Atmospheres*, **113**.

Fromm, M., and Coauthors, 2010: THE UNTOLD STORY OF PYROCUMULONIMBUS. *Bulletin of the American Meteorological Society*, **91,** 1193-1209.

Fromm, M., and Coauthors, 2008b: Stratospheric impact of the Chisholm pyrocumulonimbus eruption: 2. Vertical profile perspective. *Journal of Geophysical Research-Atmospheres*, **113**.

Peterson, D. A., E. J. Hyer, J. R. Campbell, J. E. Solbrig, and M. D. Fromm, in revision,b: A Conceptual Model for Development of Intense Pyroconvection in Western North America. *Monthly Weather Review*.

*Peterson, D. A., M. D. Fromm, J. E. Solbrig, E. J. Hyer, M. L. Surratt, and J. R. Campbell, in revision, a: **Detection and Inventory of Intense Pyroconvection in Western North America using GOES-15 Daytime Infrared Data**. *Journal of Applied Meteorology and Climatology*.

Peterson, D. A., E. J. Hyer, J. R. Campbell, M. D. Fromm, J. W. Hair, C. F. Butler, and M. A. Fenn, 2015: THE 2013 RIM FIRE Implications for Predicting Extreme Fire Spread, Pyroconvection, and Smoke Emissions. *Bulletin of the American Meteorological Society*, **96,** 229-247.

Reutter, P., and Coauthors, 2014: 3-D model simulations of dynamical and microphysical interactions in pyroconvective clouds under idealized conditions. *Atmospheric Chemistry and Physics*, **14,** 7573-7583.

Rosenfeld, D., M. Fromm, J. Trentmann, G. Luderer, M. O. Andreae, and R. Servranckx, 2007: The Chisholm firestorm: observed microstructure, precipitation and lightning activity of a pyro-cumulonimbus. *Atmospheric Chemistry and Physics*, **7,** 645-659.

Wallace, J. M., and P. V. Hobbs, 2006: *Atmospheric Science: An Introductory Survey* Second ed. Vol. 92, Academic Press.